

## SYNTHESIS AND IN VIVO INVESTIGATION OF THERAPEUTIC EFFECT OF MAGNETITE NANOFLUIDS IN MOUSE PROSTATE CANCER MODEL

J. MARKHULIA<sup>a\*</sup>, SH. KEKUTIA<sup>b</sup>, N. MITSKEVICH<sup>c</sup>, V. MIKELASHVILI<sup>b</sup>,  
L. SANEBLIDZE<sup>a</sup>, N. LELADZE<sup>c</sup>, Z. JABUA<sup>a</sup>, L. SACARESCU<sup>d</sup>,  
M. KRIECHBAUM<sup>e</sup>, L. ALMÁSY<sup>f,g</sup>

<sup>a</sup>Georgian Technical University, 77, Kostava Str., 0175, Tbilisi, Georgia

<sup>b</sup>Vladimir Chavchanidze Institute of Cybernetics of the Georgian Technical University, 5, Zurab Andzhaparidze Str., Tbilisi, Georgia

<sup>c</sup>Ivane Javakhishvili Tbilisi State University, Department of Immunology and Microbiology, 1, Chavchavadze Ave., 0179 Tbilisi, Georgia

<sup>d</sup>Petru Poni Institute of Macromolecular Chemistry Iasi, Romania

<sup>e</sup>Institute of Inorganic Chemistry, Graz University of Technology, Stremayrgasse 9/5, A-8010 Graz, Austria

<sup>f</sup>Wigner Research Centre for Physics, Institute for Solid State Physics and Optics, Hungarian Academy of Sciences, Konkoly-Thege Miklós út 29-33, Budapest-1121, Hungary

<sup>g</sup>State Key Laboratory of Environment-friendly Energy Materials, Southwest University of Science and Technology, Mianyang 621010, China

Nanofluids containing superparamagnetic iron oxide nanoparticles (SPIONs) stabilized with a biocompatible polymer polyethylene glycol (PEG) of molecular weight 4000 were synthesized by suitable modification of the standard synthetic procedure with a controlled co-precipitation technique in one-pot approach in a vacuum environment. The obtained samples were characterized using X-ray diffraction (XRD), Fourier Transform Infrared Spectroscopy (FTIR), Small-Angle X-ray Scattering (SAXS), Transmission Electron Microscopy (TEM) and Vibrating Sample Magnetometry (VSM). The therapeutic effect of magnetic nanofluids containing bare and PEG-coated magnetite nanoparticles has been studied in either monotherapy or combined therapy with anticancer drug mitoxantrone in mouse prostate cancer model. The therapeutic effect was the strongest in combined use of mitoxantrone with magnetite nanoparticles.

(Received August 6, 2018; Accepted November 7, 2018)

**Keywords:** Iron oxide nanoparticles, Prostate cancer, Mitoxantrone, Nanomedicine

### 1. Introduction

Cancer is the most terrible disease, which for several centuries (starting from Ancient Egypt 1600 BC) has become an invincible enemy of humanity [1-2]. In the 21st century, this disease still remains the main unsolved medical condition not only for biomedicine but for the entire scientific community. Despite the numerous successes of modern medicine, the complete elimination of unwanted processes in the body and re-establishing its normal functions remains a problem. The incomplete understanding of tumor biology, insufficient awareness of the sensitivity of flora and the high toxicity of anticancer agents are the reasons for search of new effective therapeutic methods in this field.

Prostate cancer is the second most frequently occurring tumor after skin cancer. It is also the second leading cause of cancer death together with lung cancer. Statistics vary between different geographic regions and ethnic groups. Although in recent years, early diagnosis has

\*Corresponding authors: j.markhulia@gtu.ge

improved and new methods of complex therapy have been discovered, the existing statistics remain unchanged [3-5]. For the treatment of prostate cancer, standard options are used, such as surgical intervention, radiotherapy, hormone therapy, also known as androgen fever (ADT) therapy, chemotherapy or a combination of these options [6-7].

The most promising and popular alternative to existing traditional methods of oncology is the application of achievements of nanotechnology [5]. The main goals are to improve both the therapeutic outcome and the methods of treatment and minimize the often occurring adverse consequences [8]. Nanotherapeutics studies have shown that, in comparison with conventional chemotherapeutic agents, therapeutic nanoparticles tend to efficiently deliver a chemotherapeutic drug to the pathological site, while avoiding toxicity in healthy organs and tissues due to several features like highly selective accumulation in tumors through a mechanism called the enhanced permeability and retention (EPR) effect and active cellular uptake (Fig. 1) [9-12]. The EPR effect, therefore, can help to increase the effectiveness of the targeted drug delivery, thereby reducing the necessary amount and toxicity of the drug and reducing the side effects usually associated with chemotherapy. In addition, encapsulating or conjugating anti-cancer drugs on nanoparticles or polymers can improve the solubility of the hydrophobic drugs in the aqueous physiological conditions [9, 13].

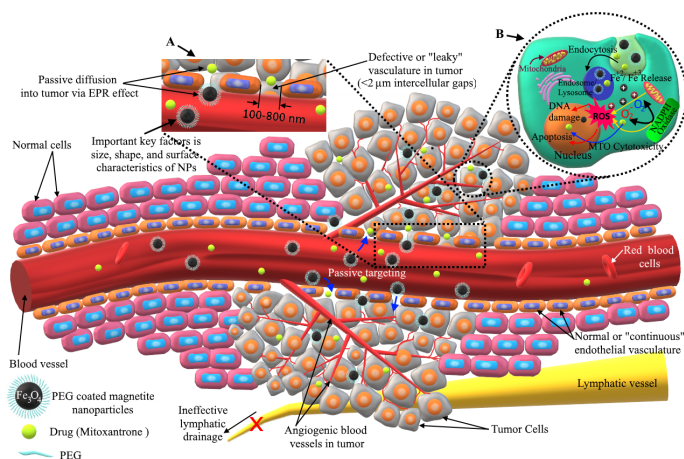


*Fig. 1. Schematic representation of the passive targeting (enhanced permeability and retention (EPR) effect) of magnetic nanoparticles and anticancer drugs. (A) Nanoparticles reach tumor cells selectively through the leaky vasculature surrounding the tumors, (B) Mechanisms of ROS induced by magnetite nanoparticles. First, NPs are internalized into the cell by endocytosis with subsequent formation of endocytotic vesicles; After that, the ions of magnetite are released from vesicles into the cell.*

Over the past decades, many types of nanoparticles have been developed and evaluated for diagnosis and therapy. Among them, the most promising and popular biomedical materials in clinical routine are nanoparticles of iron oxide (magnetite  $\text{Fe}_3\text{O}_4$  and maghemite  $\gamma\text{-Fe}_2\text{O}_3$ ) because of their suitable physicochemical and pharmacokinetic properties. Their unique magnetic properties, such as zero net magnetization, and low Curie temperature, high magnetic susceptibility, make them sensitive to external magnetic field and allows to be directed by the field gradient [14-15]. Moreover,  $\text{Fe}_3\text{O}_4$  nanoparticles (NPs) exhibit antibacterial activity due to the reactive oxygen species (ROS) [14-17], also newly formed iron ions through Fenton reactions, may significantly affect intracellular oxidation-reduction reactions and homeostasis of ROS inside tumor cells (Fig. 1) [18-21]. It should also be emphasized that magnetite nanoparticles exhibit biocompatibility, low toxicity, and environmental safety.

For the successful application of nanoparticles in biomedical applications, it is especially important to modify their surfaces by nontoxic surface layers. In this case, not only the biocompatibility is improved but also an agglomeration of nanoparticles in a physiological environment is blocked and thereby a good biodistribution and bioelimination is achieved. At the same time, the corresponding physicochemical properties are retained, for example, high

saturation magnetization, a narrow particle size distribution, and others [10,15]. Such magnetic nanoparticles can bind to drugs or various biological molecules (proteins, enzymes, antibodies or nucleotides) and due to their superparamagnetic properties, and wide choice of surface functionalities can be directed to an organ, tissue or tumor both by active and passive targeting, using an external magnetic field or without it [17,22].

The key factors affecting the efficiency of magnetic nanoparticles of iron oxide in nanotherapy, as well as the physicochemical and pharmacokinetic properties are the size, shape, size distribution and surface characteristics [9-11]. The size of the nanoparticles should be such that they can prevent rapid leakage in the blood capillaries while avoiding the capture from macrophages of the reticuloendothelial system [9,14]. Surface coating by various ligand molecules is often used for preventing particle aggregation, to ensure their stealth and increase of the life expectancy in the bloodstream [22].

Polyethylene Glycol (PEG) is one of the most frequently used polymers for modifying the surface of nanoparticles. These molecules increase the steric distance between the nanoparticles and also help to avoid the recognition by the immune system by blood leukocytes and thus prolonging the circulation of the nanoparticles in the bloodstream [16,23].

In the present work, we study the influence of two types of magnetic nanoparticles on the tumor of mouse prostate. Physicochemical properties, such as the morphology of bare and PEG-coated particles, their size distribution and magnetization have been investigated by transmission electron microscopy, small and wide angle X-ray diffraction, FT-IR spectroscopy and magnetometry. The therapeutic effect of the obtained bare and polymer-coated iron oxide nanoparticles was investigated on the tumors of the mouse prostate, either individually or combined with the antitumor drug mitoxantrone. Mitoxantrone is a synthetic derivative of anthracenedione with cytostatic (antitumor) properties, which is mainly used in the treatment of breast cancer, leukemia, lymphoma and prostate cancer. It should be noted the mechanism of the antitumor effect is not fully understood. However, it is established that the molecule can build in between the base of the DNA molecule, which leads to disruption of the replication and transcription processes and also to the blocking of topoisomerase II. MTO has a nonspecific effect on the cell cycle [24-25].

## **2. Methods and experiments**

### **2.1 Materials**

#### **2.1.1 Reagents**

All analytical reagents were used without further purification. Chemicals used for the synthesis of PEG-coated iron oxide nanoparticles were iron (III) chloride hexahydrate ( $\text{FeCl}_3 \cdot 6\text{H}_2\text{O}$ ) ( $\geq 98\%$  - Sigma-Aldrich – Germany), iron (II) sulfate heptahydrate ( $\text{FeSO}_4 \cdot 7\text{H}_2\text{O}$ ) ( $\geq 99\%$  - Carl Roth GmbH + Co. KG - Germany), ammonium hydroxide solution ( $\text{NH}_4\text{OH}$ ) ( $\geq 25\%$  - Carl Roth GmbH + Co. KG – Germany), PEG-4000 with average molar mass (M) of 3500-4500 g/mol (Carl Roth GmbH + Co. KG – Germany). Deionized water was used throughout the experiment.

#### **2.1.2 Cells RM-1**

RM-1 is a murine prostate cancer cell line, which was gifted by Virginia Commonwealth University (Richmond, VA, USA). RM-1 cells are epithelial cells of prostate tumors and are a fast-growing culture, tumor formation of about 5 mm size is obtained in a 7-day in vivo model. In the experiments, 50 000 cells / 100  $\mu\text{l}$  were taken with the injection. Tumor cells were retained in the complete PMMI 1640 culture medium, adding 10% thermoinactivated bovine serum FBS to this medium, 500  $\mu\text{l}$  of PEN-STREP, 500  $\mu\text{l}$  of sodium pyruvate, 500  $\mu\text{l}$  of MEM, a non-essential amino acid solution at 37 °C under 5 % of  $\text{CO}_2$ .

#### **2.1.3 Mitoxantrone (MTO)**

Mitoxantron dihydrochloride - 20mg/10ml solution for injection in a vial, (Pfizer, Canada Inc.) was used as an anticancer drug in this study.

#### **2.1.4 Laboratory animals**

Mice C57BL/6 is a mouse laboratory animal that has been developed and used as an inbred strain since the early stage of mouse strain development. C57BL/6 mice ("*Envigo*", Italy) were maintained at the vivarium at Iv. Javakhishvili Tbilisi State University according to standard guidelines. Design of the studies and manipulation conducted on experimental animals are reviewed and approved by the Ethics Commission (GALAS, Georgia, Tbilisi).

### **2.2 Characterization**

#### **2.2.1 Transmission electron microscopy (TEM)**

The morphology of the NPs was studied on a Hitachi High-Tech HT7700 instrument, operated in high resolution mode at 100 kV accelerating voltage. Samples have been prepared by drop casting from diluted dispersions of nanoparticles on 300 mesh holey carbon-coated copper grids (Ted Pella) and vacuum dried.

#### **2.2.2 X-ray powder diffraction (XRD)**

The dry powders of the bare magnetite and PEG-4000-modified magnetite were measured using a DRON 3M X-ray diffractometer, operating with Cu K $\alpha$  radiation ( $\lambda = 1.54178 \text{ \AA}$ ) filtered by a nickel foil, at voltage of 35 kV and current of 15 mA. The scanning speed was 2 deg/min.

#### **2.2.3 Small-angle X-ray scattering (SAXS)**

SAXS measurements were carried out using instrument SAXSpoint 2.0 (Anton Paar, Austria). Using Cu-K $\alpha$  radiation and a hybrid photon-counting 2D EIGER R series detector allowed to cover a  $q$ -range [ $0.05 \text{ nm}^{-1} - 5.7 \text{ nm}^{-1}$ ] with  $q$ -resolution  $\delta q < 0.003 \text{ nm}^{-1}$ . The measurement was carried out on samples in solution at room temperature using quartz capillaries of 1 mm in diameter. Analysis was performed with software McSAS [26], calculating particle size distribution from the scattering data.

#### **2.2.4 Magnetometry**

Magnetization curves of magnetic fluids with bare magnetite and PEG-4000 coated magnetite nanoparticles were measured on a Vibrating Sample Magnetometer (Cryogenic Limited, UK) at room temperature under an applied field up to 3 Tesla. Vibrator ran at 21 Hz and 2 mm peak to peak amplitude. 0.15 ml of nanofluids with MNPs (with a solid phase concentration of 0.66 g / 100 ml) were placed in special containers.

#### **2.2.5 FTIR spectroscopy**

The FTIR spectroscopy studies were done using an Agilent Cary 670 (Mid-IR Spectral range: 9000–350  $\text{cm}^{-1}$ ). The measurements were carried out on powder samples obtained by drying the ferrofluids containing the bare and PEG-4000 modified magnetite nanoparticles in vacuum. The samples were mixed with KBr to form pellets, and the measurements were carried out in air.

### **2.3 Synthesis of PEG coated iron oxide nanoparticles**

PEG-4000 coated SPIONs were synthesized by suitable modification of the standard synthetic procedure with a co-precipitation technique in one-pot approach in an automatic chemical reactor. Vacuum environment was used to prevent undesirable critical oxidation of Fe $^{2+}$ . 2g of PEG-4000 was diluted by 100 mL of distilled water by magnetic stirring at 40°C. Once the polymer was dissolved, it was added with a peristaltic pump to a chemical reactor filled with 0.005 mol FeSO $_4 \cdot 7\text{H}_2\text{O}$  (1.39 g) and 0.010 mol FeCl $_3 \cdot 6\text{H}_2\text{O}$  (2.71 g) powders.

After that, they are stirred by a mechanical stirrer at the temperature 40°C at 450 rpm in a vacuum environment. When the PEG and iron salts were well dissolved, 10 mL of a 0.75 M NH $_4\text{OH}$  solution was added under vigorous stirring (650 rpm) at a speed of 0.6 mL/min in vacuum (< 0.1 MPa). After formation of the black precipitates, the prepared colloidal suspension was further stirred for 1 h at 920 rpm at 45°C.

The such obtained nanofluids of PEG-coated MNPs were poured into a beaker and placed on a permanent magnet. They were washed several times with water by decanting the supernatant

in order to remove excess of chemical reaction residues and polymer. After this, the washed magnetic nanofluid was treated with an ultrasonic homogenizer for 15 minutes. The final pH was 7.5.

The fluids of bare particles were prepared in a similar way, without addition of PEG.

#### 2.4 Cancer treatment tests in mouse prostate cancer model

RM-1 murine cancer cells were stored in a growth solution at 37°C in the CO<sub>2</sub> incubator. For *in vivo* study, cells dissolved in PBS (50,000 cells/100 mL) were injected under the skin (in the neck region) in C57BL/6 mice. When the tumor size reached 5 mm, injection of magnetic nanoparticles and mitoxantrone into tumor was started: concentration of bare magnetic nanoparticles (0.04 g/100 ml) 100 µl and PEG-coating magnetic particles (concentration 0.08 g/100 ml) 100 µl, MTO (concentration: 1.25 mg/1 ml) 100 µl, each of the above solutions was administered every second day, for two weeks.

The existence of the tumor was determined by palpation (the procedure was performed in a week). Tumor growth monitoring was performed every second day by using a microcaliper. Tumor volumes (V) were calculated according to the formula:  $V = 0.5236 \times L \times W^2$ , where L is the length of tumor formation (long limb), and W is the width (short side).

The experimental animals were divided into six groups, each containing 5-7 mice, for subsequent treatment, as indicated in Table 1.

Table 1. Therapy details.

Groups	Treatment procedure
1	<i>Treatment was performed by the bare magnetite nanoparticles.</i>
2	<i>Treatment was performed by the PEG-coated magnetite nanoparticles.</i>
3	<i>Treatment was carried out by combination: bare magnetite + Mitoxantrone.</i>
4	<i>Treatment was carried out by combination: PEG-coated magnetite + Mitoxantrone.</i>
Control positive (5)	<i>Treatment was carried out by only Mitoxantrone.</i>
Control negative (6)	<i>Treatment was not performed, only PBS was administered.</i>

### 3. Results and discussion

#### 3.1 Physical characterization

The particle morphology and size distribution was revealed by transmission electron microscopy (Fig. 2). The TEM images indicate a relatively weak agglomeration of the nanoparticles. The iron oxide cores exhibit somewhat irregular shapes, varying from spherical to oval. The average size, as shown in the histogram (Fig. 2, right) is around 11.25 nm and the standard deviation 1.77 nm. The largest dimension was regarded as particle size.

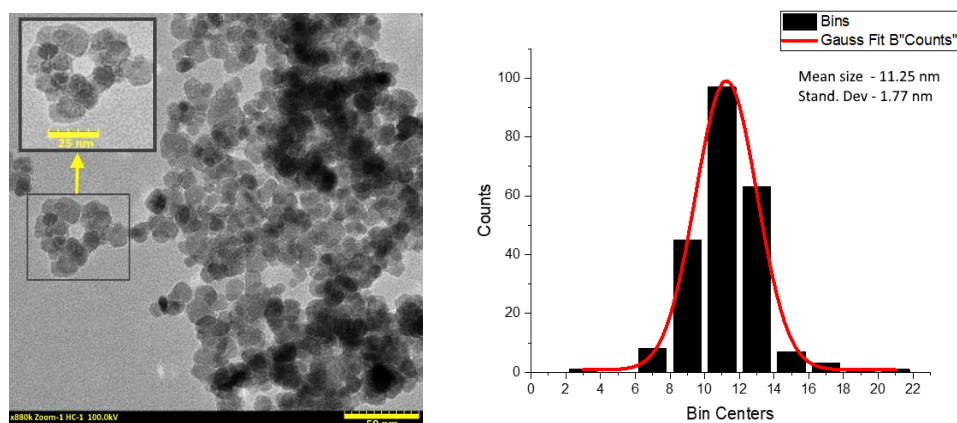


Fig. 2. The TEM image (left) and the calculated particle size distribution (right) of PEG coated  $\text{Fe}_3\text{O}_4$  NPs.

The crystalline structures and phase composition of the bare and PEG-4000 coated MNPs were determined by XRD (Fig. 4). The positions and relative intensities of all diffraction peaks fit well to those from the JCPDS file (PDF No. 65-3107) for magnetite with (220), (311), (400), (422), (551), and (440) peaks at about  $2\theta = 30.17^\circ$ ,  $35.46^\circ$ ,  $43.38^\circ$ ,  $53.69^\circ$ ,  $57.23^\circ$ , and  $62.77^\circ$ , respectively. These planes are specific to spinel cubic structure. Coating by PEG did not result in any phase change for the MNPs. All diffraction peaks show the characteristic peak broadening due to the small crystallite size of the NPs.

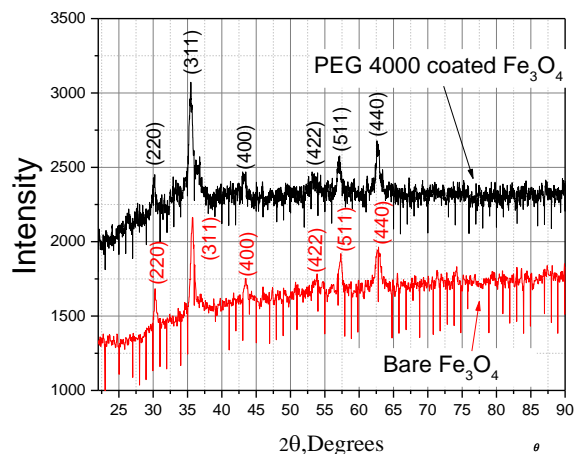


Fig. 3. XRD patterns of the bare and PEG<sub>4000</sub> coated  $\text{Fe}_3\text{O}_4$  NPs.

SAXS data revealed a polydisperse assembly of nanoparticles in the solution state. The characteristic size distribution, calculated by Monte Carlo method assuming spherical particle shape, shows a maximum of individual nanoparticles with diameters around 12 nm, and presence of agglomerated particles with cluster size up to 60 nm.

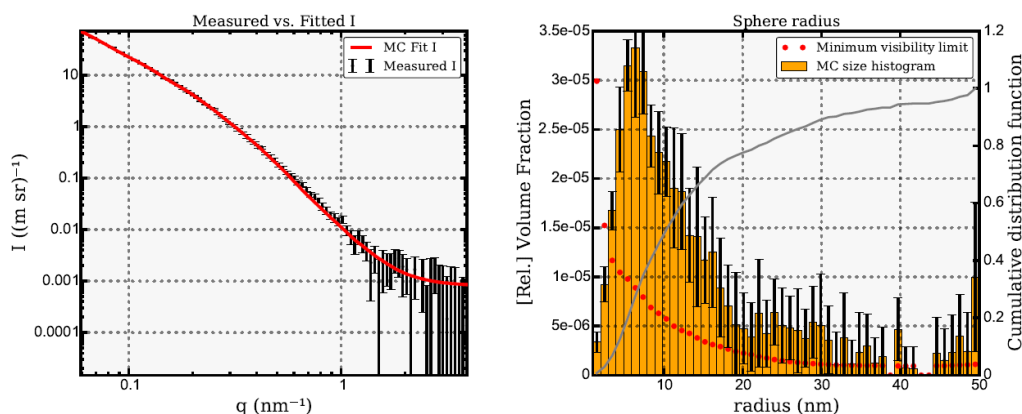


Fig. 4. Experimental SAXS curves and fit of bare  $\text{Fe}_3\text{O}_4$  NPs (left) and resulting size (volume) distribution histogram assuming spherical particle shape (right).

The magnetization curves (Fig. 5) indicate the presence of superparamagnetic nanoparticles in the synthesized nanofluids, according to the Langevin magnetization profile and the absence of hysteresis. At higher fields, the magnetization curve of sample with PEG-coated particles exhibit diamagnetic behavior with a linear decrease due to the low concentration of the magnetic particles in the studied sample [27]. In this sample, two magnetic components are observed: a paramagnetic component from the magnetic nanoparticles, and a diamagnetic one that responds linearly to the magnetic field, and originates from the dispersion medium and polymer molecules.

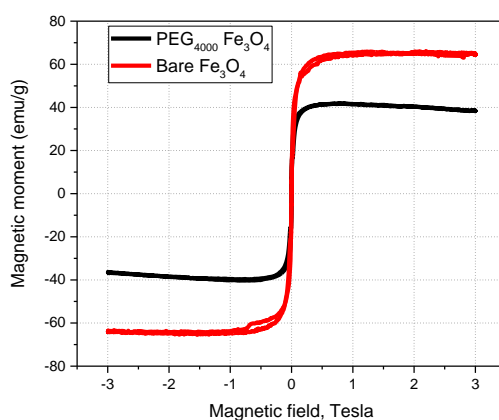


Fig. 5. Magnetization curves of bare and PEG coated  $\text{Fe}_3\text{O}_4$  NPs at 300 K.

Fig. 6 shows the FTIR spectra of pure PEG, bare and PEG-modified iron oxide nanoparticles. The bare and the polymer-modified nanoparticles show the characteristic sharp peaks at  $585 \text{ cm}^{-1}$  and  $580 \text{ cm}^{-1}$ , the fingerprint of the magnetite with a spinel structure due to the stretching vibration modes of Fe-O [28-30].

The broad absorption peaks centered on  $3430 \text{ cm}^{-1}$  (for bare magnetite) and  $3420 \text{ cm}^{-1}$  (for PEG-modified magnetite) (see Fig. 6) correspond to the O-H stretching vibrations. The appearance of these peaks in both FTIR spectra is due to the OH groups present on the surface of magnetite nanoparticles. Also on both spectra, H-O-H deformation peaks at  $1630 \text{ cm}^{-1}$  (for bare magnetite) and  $1629 \text{ cm}^{-1}$  (for PEG-modified magnetite) are observed, proving the presence of water adsorbed on the surface of  $\text{Fe}_3\text{O}_4$  [30-32].

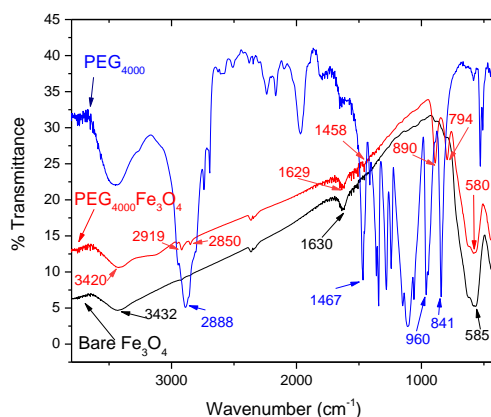


Fig. 6. FT-IR spectra of the bare magnetite NP (black curve); PEG-4000 coated magnetite NP (red curve) and pure PEG-4000 polymer (blue curve).

Additional absorption bands appear in the spectrum of the PEG-4000 modified sample, in particular, at  $2919\text{ cm}^{-1}$ ,  $2850\text{ cm}^{-1}$ ,  $1458\text{ cm}^{-1}$ ,  $891\text{ cm}^{-1}$ ,  $793\text{ cm}^{-1}$ , due to the PEG presence [0]. The  $\text{CH}_2$  vibration and bending peaks seen at  $960\text{ cm}^{-1}$  and  $841\text{ cm}^{-1}$  for the pure PEG, are blue shifted to  $890$  and  $794\text{ cm}^{-1}$ , respectively, for the PEG-coated nanoparticles, indicating the attachment of the polymer to the nanoparticle surface.

The absence of any other significant absorption bands indicates the high purity of the obtained magnetite nanoparticles, and the presence of characteristic bands of PEG in FTIR-spectra of PEG- $\text{Fe}_3\text{O}_4$  confirm the successful formation of PEGylated  $\text{Fe}_3\text{O}_4$  nanoparticles.

### 3.2 In vivo tests of magnetite nanoparticles in mouse prostate cancer model

In vivo therapeutic effect of magnetic nanofluids containing bare and polyethylene glycol-coated magnetite nanoparticles in either single or combined therapies with the chemotherapeutic drug Mitoxantrone by continuous monitoring of the tumor growth in mouse prostate cancer model was performed in six different groups. Mice C57BL/6 were injected under cutaneous by RM-1 cells (murine prostate cancer cell line). Six groups of mice selected according to the study design were injected with non- or pegylated magnetic nanoparticles carried out both separately and with combination of mitoxantrone. Injection was performed every second day for two weeks. The tumor size was measured before each injection. Upon completion of the study, mice were euthanized in accordance with the relevant ethical standards.

The results show that in groups that were treated with bare and PEG-coated magnetite nanoparticles (green and red curves), tumor growth was slowed down compared to the control (light blue curve), which indicates the therapeutic effect of magnetic nanoparticles starting from the first days of treatment.

As for pure mitoxantrone treatment, its therapeutic effect appeared on the 11th day (yellow curve), with a sharp decrease in the size of the tumor. It is noteworthy that the efficiency of MTO was increased from the first days used in combination with the bare magnetite nanoparticles (pink curve) and also with PEG-coated nanoparticles (blue curve).

The results show that the magnetic nanoparticles in combination with mitoxantrone increase the efficiency of the chemotherapeutic drug. This improvement is observed to be stronger for the PEG-4000 coated magnetite: the therapeutic effect (decreasing of the tumor size) begins on the 5th day of treatment and continues until the end of the study (11 days), compared to the bare magnetite plus mitoxantrone, for which the effects started on the 9th day. Based on these observations, it can be said that the PEG-4000 coated magnetite nanoparticles increased markedly the efficiency of MTO and showed a stronger therapeutic effect compared to bare magnetite nanoparticles. Consequently, based on the present *in vivo* study, it can be concluded that magnetite nanoparticles increase the efficacy of chemotherapy in the mouse prostate cancer model.

The therapeutic effect of magnetic nanofluids containing unstabilized and pegylated magnetite nanoparticles in the absence of MTO has been also observed in mouse prostate cancer

model. Fig. 7 shows the retarding effect of approximately similar strength of the pegylated and bare nanoparticles on the tumor growth (red and green curve), with an approximately five-fold decrease of the tumor volume compared to the control.

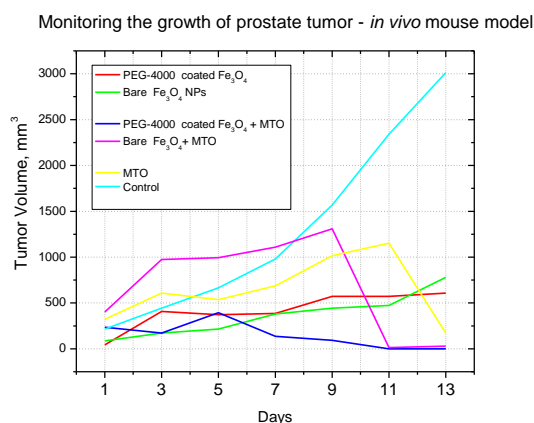


Fig. 7. Monitoring of the growth of prostate tumor *in vivo* mouse model. Magnetic nanoparticles (MNP) and chemotherapeutic mitoxantrone (MTO) were used in combination or separately.

#### 4. Conclusions

In this study, we successfully synthesized magnetic nanofluids based on bare and pegylated magnetite nanoparticles. Their magnetic, structural and morphological properties indicated a good dispersion and stability in the aqueous medium, and also their superparamagnetic nature at room temperature.

The therapeutic effect of the obtained bare and polymer-coated iron oxide nanoparticles on mouse prostate tumors, applied either individually or combined with mitoxantrone, was compared in *in vivo* tests. The results revealed the advantage of combined therapy (MNP + chemotherapy) in comparison with monotherapy (only chemotherapy), indicating a synergistic effect of iron oxide nanoparticles with a chemotherapeutic drug. This allows to reduce the drug dose and side effects, and, as a consequence, to improve tumor therapy.

#### Acknowledgments

This work was supported by the Shota Rustaveli National Science Foundation (Grant No. PhDF2016\_59). The authors acknowledge the CERIC-ERIC Consortium for the access to experimental facilities and financial support (Proposal number: 20177016).

#### References

- [1] S. I. Hajdu, *Cancer* **117**(5), 1097 (2011).
- [2] A. Karpozilos, N. Pavlidis, *European Journal of Cancer* **40**(14), 2033 (2004).
- [3] S. Dürr, C. Janko, S. Lyer, P. Tripal, M. Schwarz, J. Zaloga, R. Tietze, C. Alexiou, *Nanotechnology Reviews* **2**(4), 395 (2013).
- [4] R. L. Siegel, K. D. Miller, A. Jemal, *CA: A Cancer Journal for Clinicians* **65**(1), 5 (2015).
- [5] R. L. Siegel, K. D. Miller, A. Jemal, *CA: A Cancer Journal for Clinicians* **68**(1), 7 (2018).
- [6] S. Senapati, A. K. Mahanta, S. Kumar, P. Maiti, *Signal Transduction and Targeted Therapy* **3**, art. no. 7 (2018).
- [7] H. Signy (Editor), *Treating advanced prostate cancer. Part II. Treatment. Prostate Cancer*

- Foundation of Australia 2014.
- [8] V. T. DeVita Jr., S. A. Rosenberg, *The New England Journal of Medicine* **366**(23), 2207 (2012).
- [9] D. Rosenblum, N. Joshi, W. Tao, J. M. Karp, D. Peer, *Nature Communications* **9**(1), 1410 (2018).
- [10] H. Maeda, H. Nakamura, J. Fang, *Advanced Drug Delivery Reviews* **65**(1), 71 (2013).
- [11] F. Reyes-Ortega, A. V. Delgado, E. K. Schneider, B. L. Checa Fernández, G. R. Iglesias, *Polymers*, **10**(1), 10 (2018).
- [12] N. Bertrand, J. Wu, X. Xu, N. Kamaly, O. C. Farokhzad, *Advanced Drug Delivery Reviews* **66**, 2 (2014).
- [13] S. C. Baetke, T. Lammers, F. Kiessling, *The British Journal of Radiology* **88**(1054), 20150207 (2015).
- [14] J. Markhulia, Sh. Kekutia, Z. Jabua, V. Mikelashvili, L. Saneblidze, *SGEM Conference Proceedings* **17**(61), 51 (2017).
- [15] A. Khorramdoust, M. Ashoor, K. Saberyan, A. Eidi, *Digest Journal of Nanomaterials and Biostructures* **12**(3), 909 (2017).
- [16] A. B. Chinen, Ch. M. Guan, J. R. Ferrer, S. N. Barnaby, T. J. Merkel, Ch. A. Mirkin, *Chemical Reviews* **115**(19), 10530 (2015).
- [17] A. Mandal, S. Sekar, N. Chandrasekaran, A. Mukherjee, T. P. Sastry, *Proceedings of the Institution of Mechanical Engineers, Part H: Journal of Engineering in Medicine* **227**(11), 1224-1230 (2013).
- [18] A. Mukhopadhyay, N. Joshi, K. Chattopadhyay, G. De, *ACS Applied Materials and Interfaces* **4**(1), 142 (2012).
- [19] G. Huang, H. Chen, Y. Dong, X. Luo, H. Yu, Z. Moore, E. A. Bey, D. A. Boothman, J. Gao, *Theranostics*, **3**(2), 116 (2013).
- [20] A. Abdal Dayem, M. K. Hossain, S. B. Lee, K. Kim, S. K. Saha, G.-M. Yang, H. Y. Choi, S.-G. Cho, *International Journal of Molecular Science* **18**(1), 120 (2017).
- [21] M. Ye, Y. Han, J. Tang, Y. Piao, X. Liu, Z. Zhou, J. Gao, J. Rao, Y. Shen, *Advanced Materials* **29**(38), 1702342 (2017).
- [22] L. He, W. Xu, X. Wang, C. Wang, J. Ding, X. Chen, *Biomaterials Science* **2018**(6), 1433 (2018).
- [23] C. O. Ehi-Eromosele, B. I. Ita, E. E. J. Iweala, *Digest Journal of Nanomaterials and Biostructures* **11**(1), 7 (2016).
- [24] M. G. Krukemeyer, V. Krenn, M. Jakobs, W. Wagner, *Journal of Surgical Research* **175**(1), 35 (2012).
- [25] A. Hornung, M. Poettler, R. P. Friedrich, B. Weigel, S. Duerr, J. Zaloga, I. Cicha, C. Alexiou, C. Janko, *Anticancer Research* **36**(6), 3093 (2016).
- [26] I. Bressler, B. R. Pauw, A. F. Thünemann, *Journal of Applied Crystallography* **48**(3), 962 (2015).
- [27] J. Markhulia, V. Mikelashvili, Sh. Kekutia, L. Saneblidze, Z. Jabua, D. Daraselia, D. Jafaridze, *Journal of Pharmaceutical and Applied Chemistry* **2**(2), 33 (2016).
- [28] C. C. Wu, Y. C. Li, Y. R. Wang, T. K. Li, N. L. Chan, *Nucleic Acids Research* **41**(22), 10630 (2013).
- [29] F. Márquez, G. M. Herrera, T. Campo, M. Cotto, J. Ducongé, J. M. Sanz, E. Elizalde, *Nanoscale Research Letters* **7**(1), 210 (2012).
- [30] M. Mahdavi, M. Bin Ahmad, M. J. Haron, F. Namvar, B. Nadi, M. Z. Ab Rahman, J. Amin, *Molecules* **18**(7), 7533 (2013).
- [31] V. Panwar, P. Kumar, A. Bansal, S. S. Ray, S. L. Jain, *Applied Catalysis A: General* **498**, 25 (2015).
- [32] A. Alemdar, N. Güngör, O. I. Ece, O. Atici, *Journal of Materials Science* **40**(1), 171 (2005).